New insights in the performance and reuse of rGO/TiO_2 composites for the photocatalytic hydrogen production

Juan Corredor, María J. Rivero, Inmaculada Ortiz *

Department of Chemical and Biomolecular Engineering, ETSIIT, University of Cantabria, Avda. de los Castros s/n, 39005, Santander, Spain

* Corresponding author. E-mail address: inmaculada.ortiz@unican.es (I. Ortiz)

Keywords: rGO/TiO_2; hydrogen production; photocatalysis; photocatalyst stability.

Abstract

The viability of the photocatalytic hydrogen production is closely related to the performance and long term stability of the photocatalyst. In this work rGO/TiO_2 composites have been synthetized with graphene oxide (GO) ratios from 1% to 10% and experimentally assessed towards hydrogen generation from methanol solutions. The performance of the composite with 2% of rGO (2GT) has been compared to bare TiO_2 working with 20% volume methanol solution. The hydrogen production initial rate showed similar values with both photocatalysts decreasing after about 24 h. Further analysis of the photocatalytic process at longer times showed the negative influence of hydrogen accumulation in the reaction system. Thus, an experimental procedure with argon purge was developed and the behavior of TiO_2 and 2GT photocatalysts was compared. It is concluded that TiO_2 keeps its activity after 8 operation cycles while 2GT performance reduces progressively. This can be attributed to the further reduction of GO and the increase of defects in its structure.

1. Introduction

In the current global energy context of fossil fuel shortage and the need to mitigate climate change and the associated greenhouse gas emissions, the research and development of new and cleaner energy alternatives must be promoted. In this context, hydrogen appears as a promising clean energy vector [1–3]. Currently, about 95% of hydrogen is produced by steam reforming of natural gas under high temperatures and pressures. The remaining 5% is generated from electrolysis and from biofuels reforming. The recovery of hydrogen from the upgrading of organic wastes and from biomass, although a minor source, could contribute to increase hydrogen availability at the same time that environmental benefits are derived. Photocatalysis is among the alternatives to the recovery of hydrogen from organic liquid wastes with low-moderate energy consumption [4,5]. However, research efforts should be devoted to increase the process performance and stability.

Since the first work by Fujishima and Honda [6] on photoelectrochemical water-splitting cell for H_2 production (1972), the topic has attracted the attention of many researchers [7,8]. The low hydrogen yield associated to water splitting led to the use of sacrificial agents and photocatalysts aimed at increasing the process performance. In a recent review the state of the art and future prospectives on the photocatalytic hydrogen generation have been thoroughly analysed. The photocatalytic hydrogen production systems are classified as heterogeneous, homogeneous and hybrid systems. Among them, heterogeneous systems are closer to large-scale application because they offer longer operation times and facilitate the photocatalyst recovery after treatment [7]. TiO_2 has been one of the most studied heterogeneous photocatalysts due to its suitable properties as chemical and thermal stability,

high photoreactivity and low cost [9]. However, its wide band gap (3.2 eV) and the high recombination rate of the electron-hole pairs reduce its photocatalytic activity limiting its application. In order to improve the photocatalytic activity of TiO_2 different strategies have been developed [8]. One of them is doping the photocatalyst with different elements that will be incorporated in the TiO_2 lattice [10,11]. Attaching noble metals such as platinum to semiconductor photocatalysts leads to high hydrogen production rates because the Schottky barrier is formed in the metal/semiconductor interface and the recombination rate is reduced [12–14]. However, the scarcity and high price of noble metals limit its application. Currently, other strategies such as the use of earth-abundant metals as cocatalyst, and heterojunction structures, e.g., Z-scheme between two semiconductors, can effectively facilitate charge transfer and reduce the recombination of photogenerated electrons and holes, enhancing photocatalytic performance. Heterojunction catalysts composed of graphitic carbon nitride (g-C_3N_4) instead of TiO_2 have attracted increasing attention for hydrogen production under visible light [15–18] as well as the use of carbonaceous composite materials [19,20].

In this way, synthesis of composite photocatalysts incorporating graphene oxide (GO) appears as an interesting alternative. GO is a two-dimensional planar sheet composed by localized sp^3 defects within the sp^2 bonded carbon atoms structured in a honeycomb shaped network with binded oxygenated groups. It can be reduced to graphene which has excellent electrical conductivity and large surface area. These properties can improve the photocatalytic activity of the TiO_2 reducing the electron-hole recombination rate thanks to the ability of the graphene to carry charges due to its fermi level being lower than the TiO_2 conduction band [21–23].

In this work, rGO\TiO_2 composites have been synthesized for the photocatalytic hydrogen generation from methanol solutions. After analysis and optimization of the concentration of GO in the composite the performance and stability of the photocatalysts was studied for long operation times.

2. Materials and methods

2.1. Materials

HPLC grade methanol was provided by Scharlau and isopropanol 99.5% was supplied by Acros Organics. TiO_2 P25 was purchased to Evonik, and a dispersion of graphene oxide sheets in water solvent with 4 mg mL^{-1} GO was supplied by Graphenea. Pure argon 3X was provided by Praxair.

2.2. Photocatalyst preparation and characterization

rGO/TiO_2 composites with 1, 2, 5 and 10% of rGO weight were synthesized following the hydrothermal method described in previous works [22].

The materials characterization was carried out with different techniques. Fourier transform infrared spectra (FTIR) were recorded in a Spectrum Two spectrometer (PerkinElmer). Thermogravimetric analysis were performed in a Shimadzu DTG-60H Differential Thermal Gravimetric Analyzer by heating the samples in nitrogen atmosphere (50 mL/min) from 25 ºC to 800 ºC at 10 ºC min^{-1}. Raman spectra were recorded by Horiba T64000 Raman Spectrometer with a 514.5 nm laser of Kr-Ar and an effective power of 5mW on the sample. The specific surface area of the photocatalysts was measured by the Brunauer-Emmett-Teller

(BET) method from nitrogen adsorption-desorption data in a Micromeritics ASAP 2000 equipment.

2.3 Hydrogen production

The photocatalytic hydrogen production experiments aimed at comparing the performance of the composite catalysts with different rGO/TiO_2 weight ratios were carried out in a sealed 225 mL borosilicate photoreactor with 180 mL of 20% vol. methanol solution and 0.10 g/L of photocatalyst. The photocatalyst long time performance experiments were carried out in a 330 mL borosilicate photoreactor using 240 mL of 20% vol. methanol solution as sacrificial agent and 0.18 g/L of photocatalyst. The photoreactor was connected to a gas chromatograph Shimadzu 2010 Plus equipped with a thermal conductivity detector and a Shin Carbon ST 80/100 column using argon as carrier gas. 4 Philips PL-S 9W lamps, that operated within a wavelength range between 315 and 400 nm and a maximum emission at 365 nm, were used as light source. The irradiance was 7.5 $W \cdot m^{-2}$, measured with a Delta Ohm HD 2102.1 photoradiometer.

Argon was bubbled through the suspension for 30 min in the dark to remove oxygen before the reaction. The temperature was 20 ºC.

3. Results

3.1. Photocatalysts characterization

TGA curves of TiO_2 and rGO/TiO_2 photocatalysts are shown in Fig. 1. The GO thermogravimetric curve showed 3 different mass loss steps. The first step up to 100 ºC corresponded to the adsorbed water in the material. From 150 to 300 ºC, the mass loss was

due to the removal of the oxygen-containing groups. Finally, the mass loss from 500 ºC on was attributable to the destruction of the carbon skeleton of graphene oxide. Within these data the content of GO in the composites was determined as shown in Table 1.

Catalyst code	1GT	2GT	5GT	10GT
Theoretical rGO (%)	1	2	5	10
Measured rGO (%)	3.4	3.9	6.8	11.8

Table 1. GO content in the composites determined thought TGA.

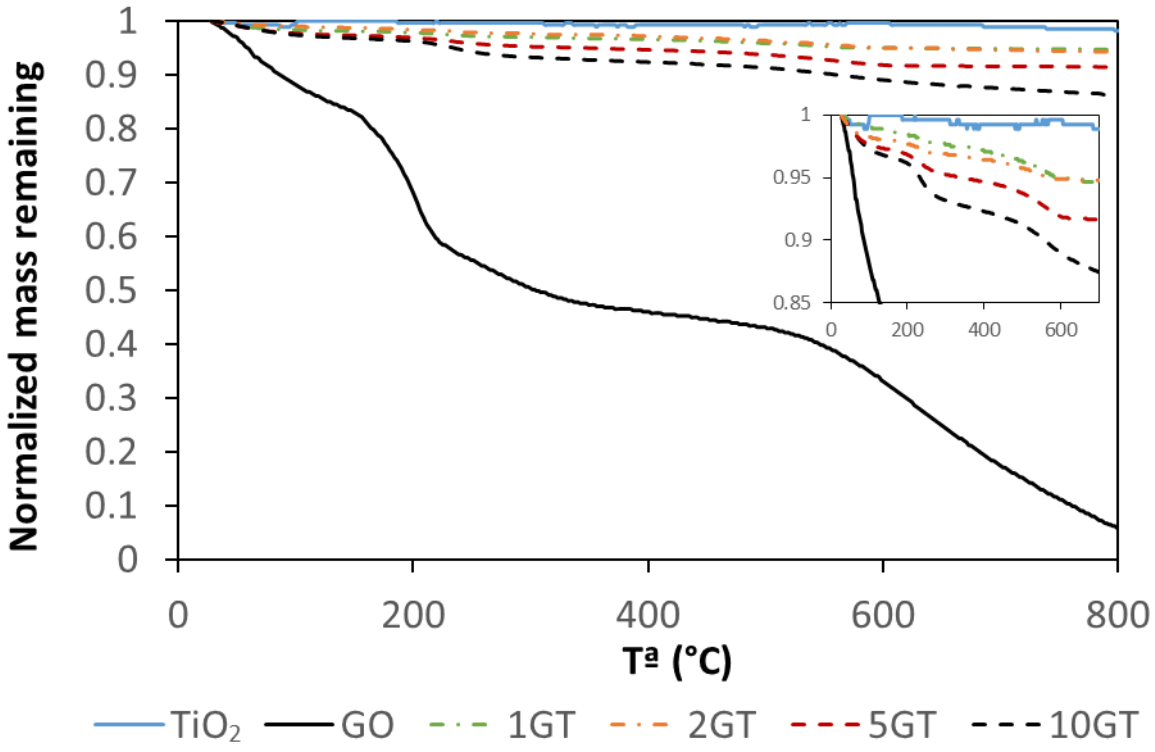

Figure 1. TGA of the synthesized photocatalysts with different rGO/TiO_2 weight ratio.

FTIR spectra of TiO_2 and 2GT before and after the photocatalytic experiments and FTIR spectrum of GO were obtained (Fig. 2). The 3400 cm^{-1} band was assigned to the stretching vibration of the O-H groups of water. The bands at 1720 and 1619 cm^{-1} in the GO spectrum

were assigned to C=O stretching vibrations from carbonyl and carboxylic groups, and C=C stretching vibrations respectively. 1380, 1161 and 1037 cm^{-1} bands were attributed to C-O stretching vibrations in GO. In 2GT spectrum, bands of C=O groups did not appear, indicating a successful reduction of GO during the hydrothermal process. All composite materials presented intense bands at 500–800 cm^{-1} that were attributed to the stretching vibrations of Ti–O–Ti [20].

The materials were also characterized after 96 h of experiment. For the recycled 2GT, C=C band shifted to lower wavenumbers in comparison to the fresh photocatalysts [24]. This could be attributed to the modification of the photocatalyst structure during the photocatalytic process. In addition, the recycled photocatalysts showed intense bands at 1200 and 1150 cm^{-1} that were assigned to C-F stretching vibrations from the polytetrafluoroethylene (PTFE) released from the magnetic stirring bar during the photocatalytic process [25].

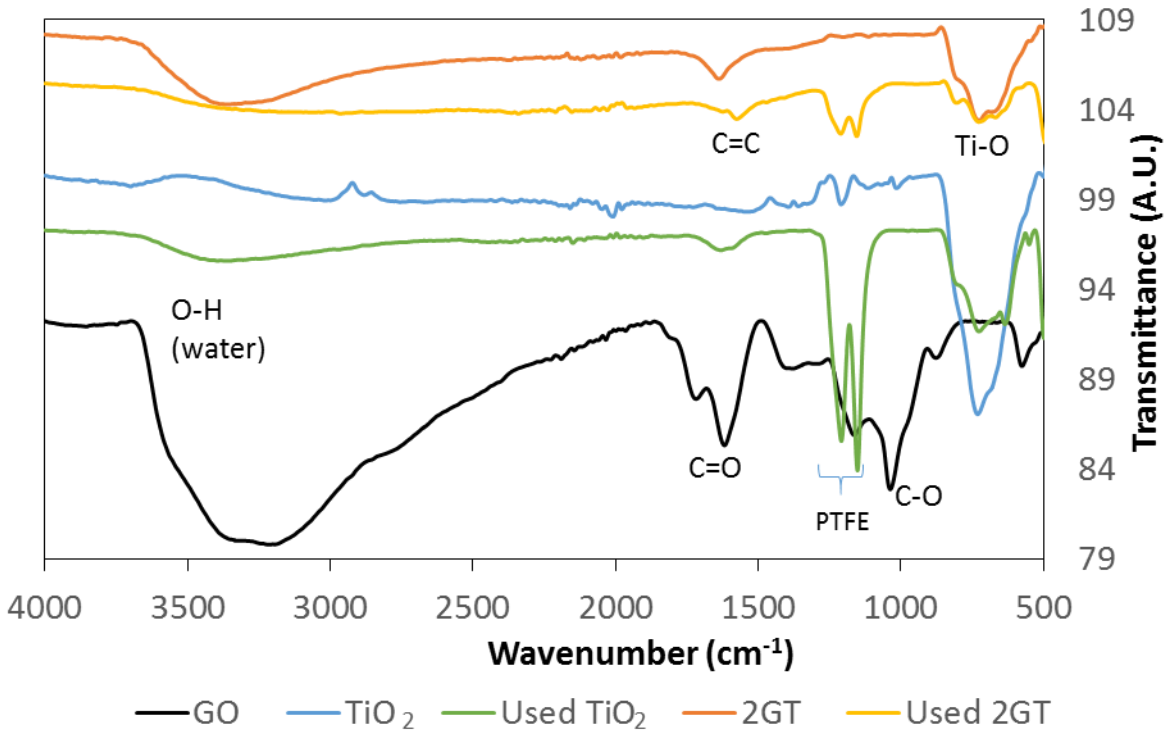

Figure 2. Photocatalysts FTIR spectra before and after the photocatalytic process.

Figure 3 shows Raman spectra of GO and fresh and recycled photocatalysts. TiO_2 Raman spectrum showed strong bands at 140, 397, 515 and 635 cm^{-1} which corresponded to E_g, B_{1g}, A_{1g} and E_g lattice vibrations of Ti and O atoms in the anatase unit cell [26]. No differences were found when comparing fresh and recycled photocatalysts suggesting that TiO_2 preserved its structure during the hydrothermal synthesis and after the photocatalytic hydrogen production process.

The band at 1353 cm^{-1} corresponds to D bands of reduced graphene oxide. The bands G and D' were found from the deconvolution through a Lorenzian fitting of the band that appeared around 1600 cm^{-1} (Table 2). These bands corresponding to reduced graphene oxide confirmed its presence in the composite. The recycled 2GT, showed a noticeable blue shift ($\approx$ 15 cm^{-1}) in the G band position. This fact could be attributed to changes in the rGO structure. The ratio I_D/I_G increased in comparison to the fresh composite showing a higher number of defects in the rGO sheets which can be caused by a further reduction of the rGO sheets (Table 2). This fact was also observed by Sher Shah *et. al* in the degradation of Rhodamine B using rGO/TiO_2 photocatalyst [27]. In addition, after the photocatalytic process the composite colour became darker as it can be observed in Figure 4, which suggests again that 2GT suffered a reduction during the photocatalytic hydrogen production reaction. This reduction could be caused by the electron transfer from the TiO_2 conduction band to rGO.

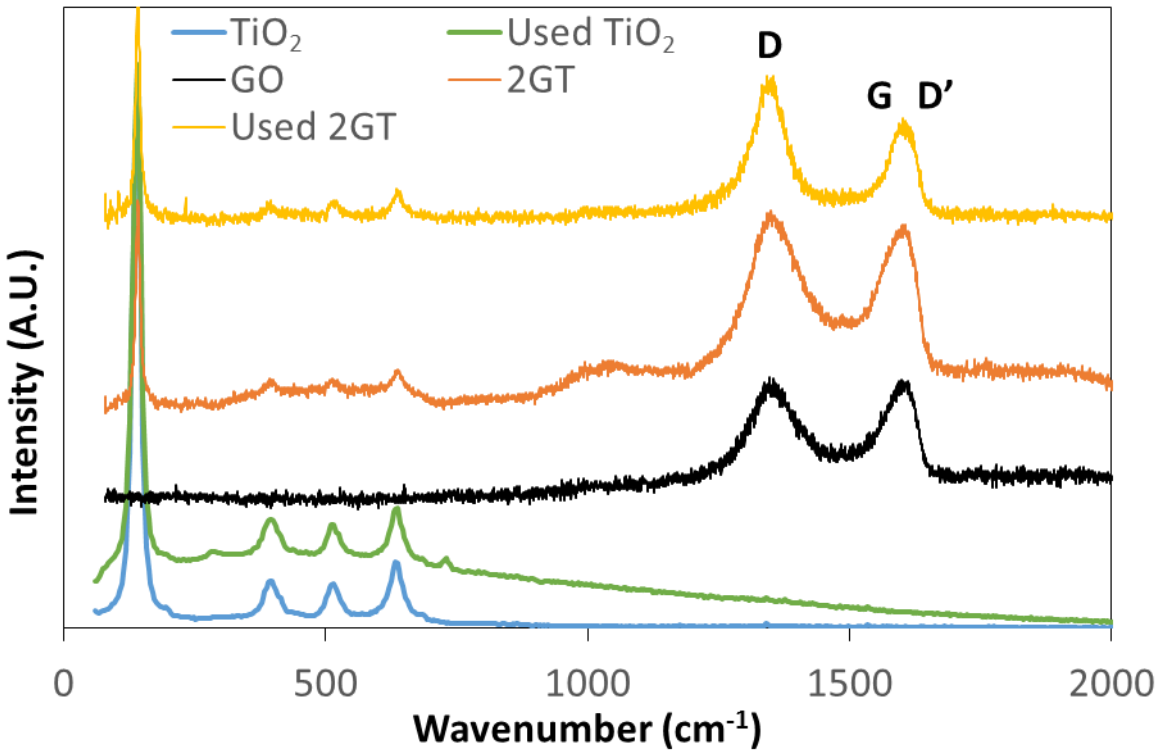

Figure 3. Raman spectra of fresh and recycled photocatalysts, and GO.

	D (cm^{-1})	G (cm^{-1})	D' (cm^{-1})	I_D/I_G
GO	1355	1580	1610	1.63
Fresh 2GT	1355	1580	1610	1.66
Recycled 2GT	1350	1595	1618	1.86

Table 2. D, G and G' bands position and I_D/I_G.

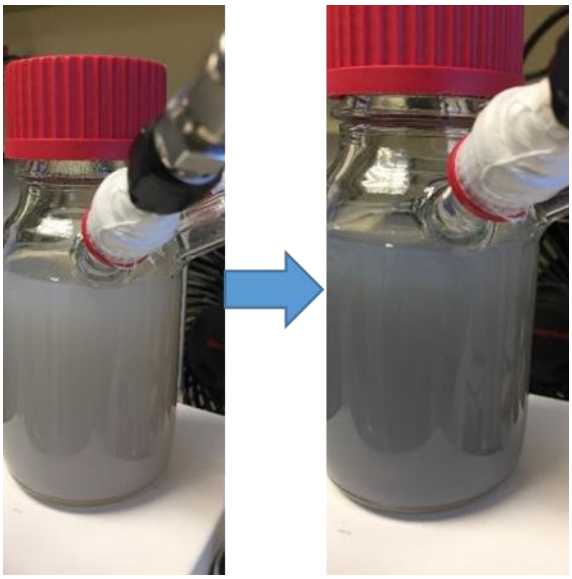

Figure 4. 2GT suspension before (left) and after (right) the photocatalytic hydrogen production.

BET specific surface areas of bare TiO_2 and the composites are shown in Table 3. An increase in the specific surface area was observed in the composites in comparison with bare TiO_2, due to the presence of the reduced graphene oxide sheets. Moreover, the specific surface area increases with GO content in the catalysts, which is in agreement with the literature [26, 27]. However, photocatalytic hydrogen production not only depends on the surface area of the catalyst. Therefore, a straight relationship between both variables has not been proposed.

Catalyst code	**TiO_2**	**1GT**	**2GT**	**5GT**	**10GT**
Specific surface area (m^2 g^{-1})	54.99 ± 0.29	57.70 ± 0.27	62.63 ± 0.15	77.79 ± 0.31	79.60 ± 0.31

Table 3. Specific surface area of the photocatalysts

Considering the optical properties, band gap analyses for these catalysts have been previously reported in Ribao et al. 2018 [22]. A shift to less energy was observed in the composite band

gap. Nevertheless, this behavior is not related to the results of this manuscript as they have been obtained working only with UV light.

3.2. Photocatalyst performance

3.2.1. Performance of the composite photocatalysts

Two Preliminary experiments, one with 20% vol. methanol solution in the absence of catalyst and the second one with photocatalyst in the absence of sacrificial agent, were carried out under UV irradiation to check the unlikely generation of hydrogen. In both cases no hydrogen production was detected.

As mentioned in the previous section after synthesis of the composites, they were tested for the photocatalytic hydrogen production (Fig. 5). The catalyst concentration was 0.1 g L^{-1} and the experiments lasted for 5 h. 2GT and 1GT showed similar hydrogen production with a maximum value of 40 µmol $g_{catalyst}^{-1}$. However, 5GT and 10GT performed lower hydrogen production. The presence of rGO can lower the charge carrier recombination rate in the photocatalyst because the photogenerated electrons on the conduction band can migrate from the TiO_2 to rGO improving the photocatalyst activity as consequence; but, on the contrary rGO sheets can reduce the number of available active sites in the photocatalyst decreasing its photoreactivity [28]. Therefore, 2GT reached the best compromise between these effects.

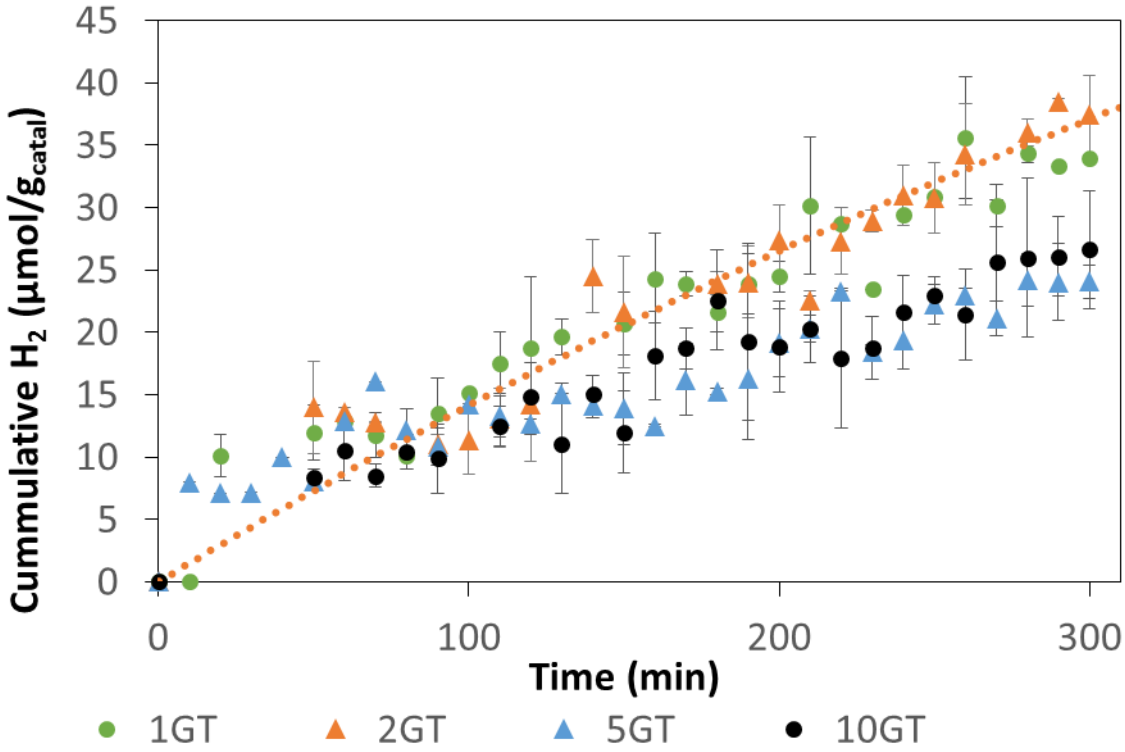

Figure 5. Hydrogen production using photocatalysts with different rGO/TiO_2 weight ratios.

3.2.2. Photocatalyst stability

The comparative performance of TiO_2 and 2GT was analyzed from the results achieved in experiments that lasted for 96 h (Fig. 6). The initial rate was very similar in both photocatalysts with a value of 1.6 µmol H_2 $g_{catalyst}^{-1}$ h^{-1}. After approximately 20 h in both experiments a progressive decrease of the hydrogen production rate was observed until the process stopped completely (plateau around 80 h). Thus, this loss of activity deserved further research as it will be detailed below.

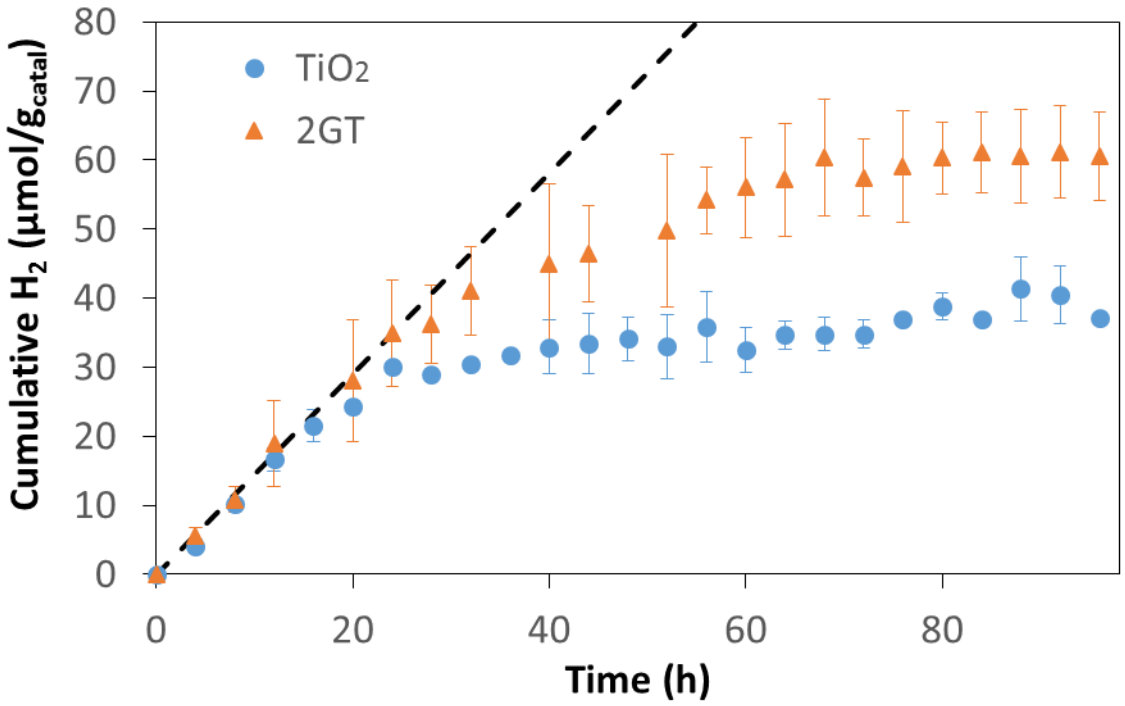

Figure 6. Hydrogen production with photocatalyst in suspension.

Next, a set of experiments with alternative periods of photocatalysis and argon purge were conducted with TiO_2 and 2GT. The results achieved after 8 cycles are shown in Figure 7. The first cycle of TiO_2 and 2GT in Figure 7 can be compared with the data corresponding to the first 12 h of both photocatalysts represented in Figure 6. In both cases, the hydrogen production values are within the experimental error. The first 5 cycles were run for 12 h each; the rate of hydrogen generation was similar for both photocatalysts. While TiO_2 kept the rate almost constant, 2GT suffered a slight decrease in the rate with the successive cycles, fact that was also observed after the 8^{th} cycle performed under similar conditions. The rate decrease could be explained by the further reduction of GO in the composite with operation time and an increase in the number of defects that are detrimental for the photocatalytic activity. The 6^{th} cycle (Figure 7) showed a similar behaviour in the hydrogen generation as

in Figure 6, that was attributed to the accumulation of hydrogen in the reaction vessel and the inhibitory effect of the reaction product as previously reported [29,30]. The difference between H^+/H_2 reduction potential and TiO_2 conduction band potential was diminished due to the accumulation of H_2 reducing the driving force until the hydrogen production stops. For long operation times (cycle 6^{th}) it is remarkable that recycled 2GT suffered a decrease in the production rate compared to the fresh catalyst that leads to less hydrogen production than for TiO_2.

Cycle 7 was performed by feeding hydrogen in order to check its inhibitory effect, and as expected no hydrogen was formed. After removal of the retained hydrogen with the argon purge the hydrogen generation rate was recovered as shown in cycle number 8.

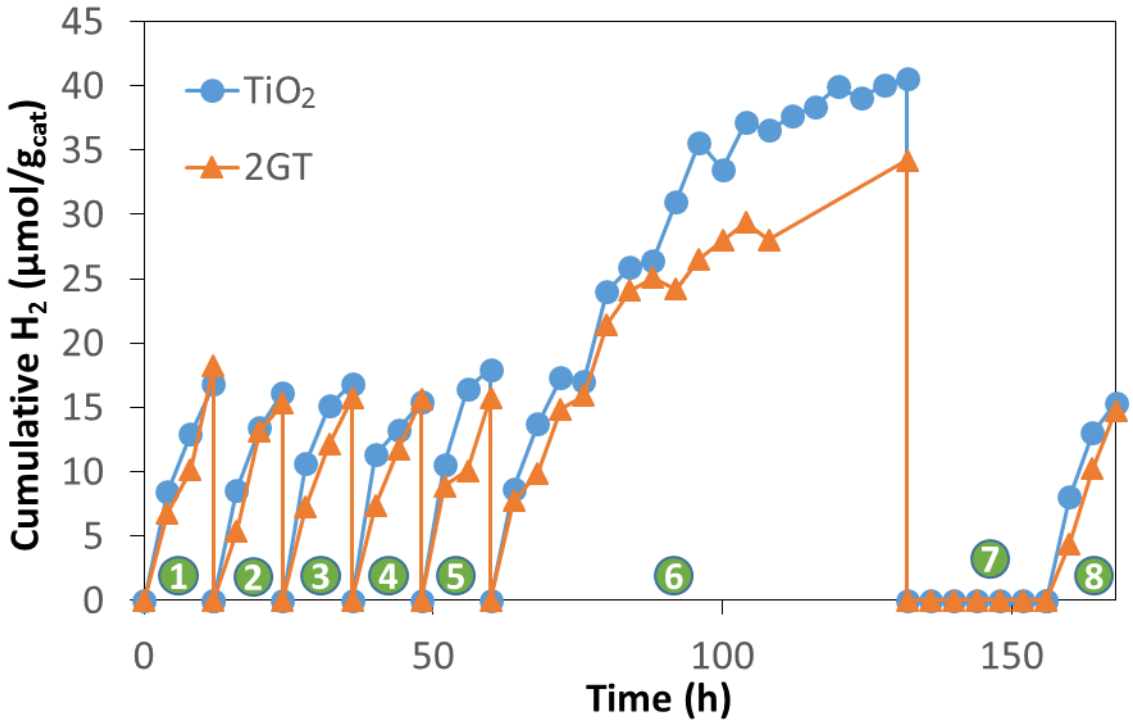

Figure 7. TiO_2 and 2GT photocatalytic hydrogen production during some cycles.

The pH was measured after each cycle. Figure 8 shows the change in this variable from the initial value of the methanol solution, 5.8. In the first cycle the sharpest decrease of pH took place, from 5.8 to 4.3 and in the second cycle from 4.3 to 4; in the successive cycles there was a slight decrease of pH that reached a value of 3.8 after the last cycle. This decrease of pH could be well attributed to the formation of formic acid produced as intermediate during the methanol decomposition as it can be observed in Eqs. (1,2,3) [31]. The pH was maintained around 3.8 because of the buffer capacity of the formic acid that smooths the pH change during the photocatalytic hydrogen production process and keeps it close to its pK_a value of 3.8 [32].

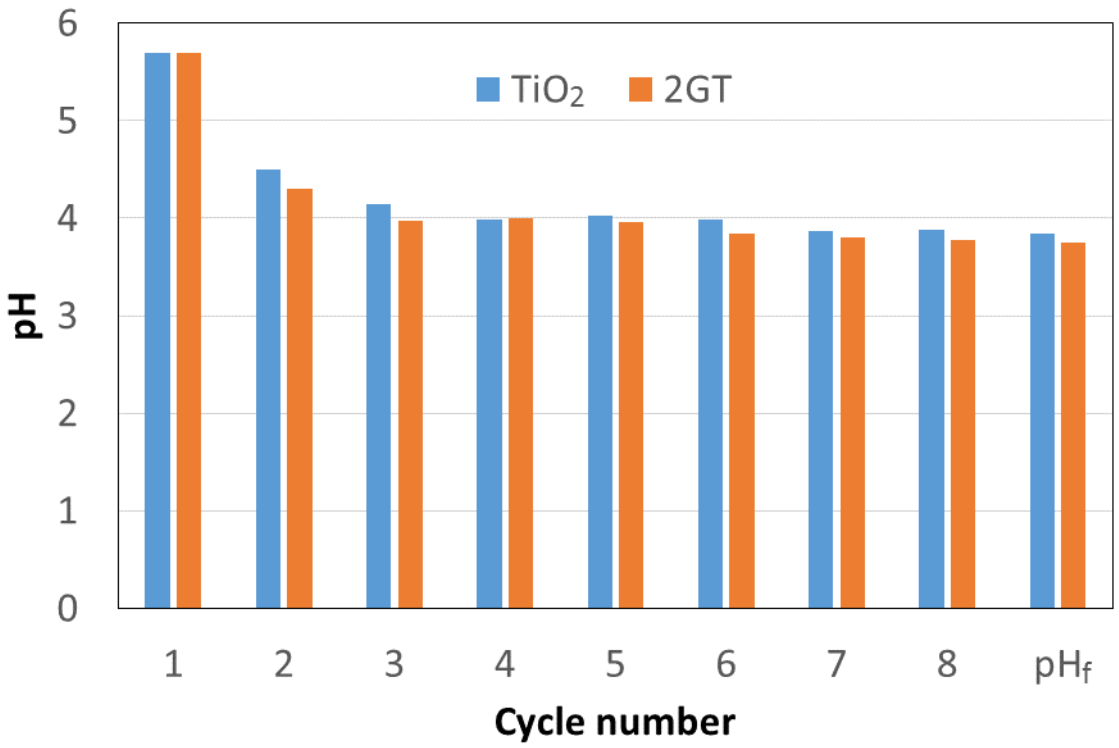

Figure 8. Initial pH in each cycle and the final pH after the 8 cycles.

The degradation mechanism of methanol is shown in Equations 1, 2, 3. This mechanism takes place by direct oxidation by the catalyst holes, which is the main oxidation pathway when the molar water/methanol ratio is lower than 300 [33].

$$CH_3OH \xrightarrow{rGO/TiO_2,\ vh} HCOH + H_2 \qquad Eq.1$$

$$HCOH + H_2O \xrightarrow{rGO/TiO_2,\ vh} HCOOH + H_2 \qquad Eq.2$$

$$HCOOH \xrightarrow{rGO/TiO_2,\ vh} CO_2 + H_2 \qquad Eq.3$$

4. Conclusions

Photocatalytic hydrogen production appears as a good opportunity when looking for sustainable energy resources at the same time that organic wastes are upgraded. The final deployment of the technology is strongly related to the availability of high performance and stability catalysts. Being TiO_2 the most widely used material, research efforts are focused on improving its main drawbacks, i.e., its wide band gap (3.2 eV) and the high recombination rate of the electron-hole pairs. The use of noble metals, although increasing the effectiveness, decrease the cost-effectiveness of the process, thus, a composite material made with TiO_2 and graphene oxide has been proposed. The presence of GO in the photocatalytic hydrogen generation was analyzed and best results were obtained with 2% of carbonaceous material.

The initial hydrogen production rates for fresh TiO_2 and 2GT catalysts were similar with a value around 1.6 μmol H_2 $g_{catalyst}^{-1}$ h^{-1}. But, the accumulation of the generated hydrogen in the photocatalytic reactor slowed down the process kinetics until it was completely stopped

255 after approximately 80 h. A protocol with argon purge in order to remove hydrogen from the
256 reaction mixture has shown effective in recovering the hydrogen generation rate for long
257 operation times

258 TiO_2 and 2GT were also evaluated in several operation cycles with argon purge after each
259 cycle. While TiO_2 kept the initial hydrogen production rate almost constant, 2GT suffered a
260 slight decrease after the successive cycles compromising its performance. This could be
261 attributed to the further 2GT reduction after each cycle and the increase in the number of
262 defects that are detrimental for the photocatalytic activity.

263

264 5. Acknowledgements

265 Financial support from projects CTM2015-69845-R (MINECO/FEDER, UE) and RTI2018-
266 099407-B-I00 (MCIU/AEI/FEDER, UE) is gratefully acknowledged. Juan Corredor is
267 grateful to a FPI contract grant (BES-2016-079201).

268 6. References

269 [1] Ruan ZH, Li YD, Yuan Y, Lin KF, Tan HP. Energy-absorption-based explanation of
270 the photocatalytic activity enhancement mechanism of TiO_2 nanofibers. Int J Hydrogen
271 Energy 2019;44:21569–76. doi:10.1016/j.ijhydene.2019.06.083.

272 [2] Sepahvand H, Sharifnia S. Photocatalytic overall water splitting by Z-scheme g-
273 $C_3N_4/BiFeO_3$ heterojunction. Int J Hydrogen Energy 2019;44:23658–68.
274 doi:10.1016/j.ijhydene.2019.07.078.

[3] Supplis C, Gros F, Dahi G, Dauchet J, Roudet M, Gloaguen F, et al. Spectral radiative analysis of bio-inspired H_2 production in a benchmark photoreactor: A first investigation using spatial photonic balance. Int J Hydrogen Energy 2018;43:8221–31. doi:10.1016/j.ijhydene.2018.03.097.

[4] Cargnello M, Montini T, Smolin SY, Priebe JB, Delgado-Jaén JJ, Doan-Nguyen VVT, et al. Engineering titania nanostructure to tune and improve its photocatalytic activity. Proc Natl Acad Sci U S A 2016;113:3966–71. doi:10.1073/pnas.1524806113.

[5] Holladay JD, Hu J, King DL, Wang Y. An overview of hydrogen production technologies. Catal Today J 2009;139:244–60. doi:10.1016/j.cattod.2008.08.039.

[6] Fujishima A, Honda K. Electrochemical photolysis of water at a semiconductor electrode. Nature 1972;238:37–8. doi:10.1038/238037a0.

[7] Corredor J, Rivero MJ, Rangel CM, Gloaguen F, Ortiz I. Comprehensive review and future perspectives on the photocatalytic hydrogen production. J Chem Technol Biotechnol 2019;94:3049–63. doi:10.1002/jctb.6123.

[8] Fajrina N, Tahir M. A critical review in strategies to improve photocatalytic water splitting towards hydrogen production. Int J Hydrogen Energy 2018;44:540–77. doi:10.1016/j.ijhydene.2018.10.200.

[9] Guan L, Chen X. Photoexcited Charge Transport and Accumulation in Anatase TiO_2. ACS Appl Energy Mater 2018;1:4313–20. doi:10.1021/acsaem.8b00944.

[10] Gao Q, Si F, Zhang S, Fang Y, Chen X, Yang S. Hydrogenated F-doped TiO_2 for photocatalytic hydrogen evolution and pollutant degradation. Int J Hydrogen Energy 2019;44:8011–9. doi:10.1016/j.ijhydene.2019.01.233.

[11] Lin J, Liu Y, Liu Y, Huang C, Liu W, Mi X, et al. SnS_2 Nanosheets/H-TiO_2 Nanotube Arrays as a Type II Heterojunctioned Photoanode for Photoelectrochemical Water Splitting. ChemSusChem 2019;12:961–7. doi:10.1002/cssc.201802691.

[12] Ribao P, Alexandra Esteves M, Fernandes VR, Rivero MJ, Rangel CM, Ortiz I. Challenges arising from the use of TiO_2/rGO/Pt photocatalysts to produce hydrogen from crude glycerol compared to synthetic glycerol. Int J Hydrogen Energy 2018;44:28494–506. doi:10.1016/j.ijhydene.2018.09.148.

[13] Lin X, Wang J. Green synthesis of well dispersed TiO_2/Pt nanoparticles photocatalysts and enhanced photocatalytic activity towards hydrogen. Int J Hydrogen Energy 2019;44:31853–9. doi:10.1016/j.ijhydene.2019.10.062.

[14] Hu H, Qian D, Lin P, Ding Z, Cui C. Oxygen vacancies mediated in-situ growth of noble-metal (Ag, Au, Pt) nanoparticles on 3D TiO_2 hierarchical spheres for efficient photocatalytic hydrogen evolution from water splitting. Int J Hydrogen Energy 2020;45:629–39. doi:10.1016/j.ijhydene.2019.10.231.

[15] Lu X, Xie J, Chen X, Li X. Engineering MPx (M = Fe, Co or Ni) interface electron transfer channels for boosting photocatalytic H_2 evolution over g-C_3N_4/MoS_2 layered heterojunctions. Appl Catal B Environ 2019;252:250–9. doi:10.1016/j.apcatb.2019.04.012.

[16] He K, Xie J, Liu Z, Li N, Chen X, Hu J, et al. Multi-funcational Ni_3C Cocatalyst/g-C_3N_4 nanoheterojunctions for robust photocatalytic H_2 evolution under Visible Light. J Mater Chem. A 2018;6:13110–22. doi:10.1039/C8TA03048K.

317 [17] Ma X, Chen C, Hu J, Zheng M, Wang H, Dong S, et al. Evidence of direct Z-scheme
318 g-C_3N_4/WS_2 nanocomposite under interfacial coupling: First-principles study. J Alloys
319 Compd 2019;788:1–9. doi:10.1016/j.jallcom.2019.02.044.

320 [18] Lu X, Xie J, Liu SY, Adamski A, Chen X, Li X. Low-Cost Ni_3B/$Ni(OH)_2$ as an
321 Ecofriendly Hybrid Cocatalyst for Remarkably Boosting Photocatalytic H2 Production over
322 g-C_3N_4 Nanosheets. ACS Sustain Chem Eng 2018;6:13140–50.
323 doi:10.1021/acssuschemeng.8b02653.

324 [19] Hafeez HY, Lakhera SK, Bellamkonda S, Rao GR, Shankar M V., Bahnemann DW,
325 et al. Construction of ternary hybrid layered reduced graphene oxide supported g-C_3N_4-TiO_2
326 nanocomposite and its photocatalytic hydrogen production activity. Int J Hydrogen Energy
327 2018;43:3892–904. doi:10.1016/j.ijhydene.2017.09.048.

328 [20] Xie H, Hou C, Wang H, Zhang Q, Li Y. S, N Co-Doped Graphene Quantum Dot/TiO_2
329 Composites for Efficient Photocatalytic Hydrogen Generation. Nanoscale Res Lett
330 2017;12:400. doi:10.1186/s11671-017-2101-1.

331 [21] Khalid NR, Majid A, Tahir MB, Niaz NA, Khalid S. Carbonaceous-TiO_2
332 nanomaterials for photocatalytic degradation of pollutants: A review. Ceram Int
333 2017;43:14552–71. doi:10.1016/j.ceramint.2017.08.143.

334 [22] Ribao P, Rivero MJ, Ortiz I. Enhanced photocatalytic activity using GO/TiO_2 catalyst
335 for the removal of DCA solutions. Environ Sci Pollut Res 2018;25:34893–902.
336 doi:10.1007/s11356-017-0901-6.

[23] Rivero MJ, Iglesias O, Ribao P, Ortiz I. Kinetic performance of TiO_2/Pt/reduced graphene oxide composites in the photocatalytic hydrogen production. Int J Hydrogen Energy 2019;44:101–9. doi:10.1016/j.ijhydene.2018.02.115.

[24] Ding YH, Zhang P, Zhuo Q, Ren HM, Yang ZM, Jiang Y. A green approach to the synthesis of reduced graphene oxide nanosheets under UV irradiation. Nanotechnology 2011;22:215601. doi:10.1088/0957-4484/22/21/215601.

[25] Wang R, Xu G, He Y. Structure and properties of polytetrafluoroethylene (PTFE) fibers. E-Polymers 2017;17:215–20. doi:10.1515/epoly-2016-0059.

[26] Šćepanović MJ, Grujić-Brojčin M, Dohčević-Mitrović ZD, Popović Z V. Characterization of anatase TiO_2 nanopowder by variable-temperature raman spectroscopy. Sci Sinter 2009;41:67–73. doi:10.2298/SOS0901067S.

[27] Sher Shah MSA, Park AR, Zhang K, Park JH, Yoo PJ. Green synthesis of biphasic TiO_2-reduced graphene oxide nanocomposites with highly enhanced photocatalytic activity. ACS Appl Mater Interfaces 2012;4:3893–901. doi:10.1021/am301287m.

[28] Cao XR, Tian GH, Chen YJ, Zhou J, Zhou W, Tian CG, et al. Hierarchical composites of TiO_2 nanowire arrays on reduced graphene oxide nanosheets with enhanced photocatalytic hydrogen evolution performance. J Mater Chem A 2014;2:4366–74. doi:10.1039/c3ta14272h.

[29] Kuang L, Zhang W. Enhanced hydrogen production by carbon-doped TiO_2 decorated with reduced graphene oxide (rGO) under visible light irradiation. RSC Adv 2016;6:2479–88. doi:10.1039/C5RA26096E.

358 [30] Choi W. Photocatalytic hydrogen production using surface-modified titania
359 nanoparticles. Sol Hydrog Nanotechnol II 2007;6650:164–72. doi:10.1117/12.737292.

360 [31] Ahmed AY, Kandiel TA, Ivanova I, Bahnemann D. Photocatalytic and
361 photoelectrochemical oxidation mechanisms of methanol on TiO_2 in aqueous solution. Appl
362 Surf Sci 2014;319:44–9. doi:10.1016/j.apsusc.2014.07.134.

363 [32] Muckerman JT, Skone JH, Ning M, Wasada-Tsutsui Y. Toward the accurate
364 calculation of pKa values in water and acetonitrile. Biochim Biophys Acta - Bioenerg
365 2013;1827:882–91. doi:10.1016/j.bbabio.2013.03.011.

366 [33] Wang CY, Groenzin H, Shultz MJ. Direct observation of competitive adsorption
367 between methanol and water on TiO_2: An in situ sum-frequency generation study. J Am
368 Chem Soc 2004;126:8094–5. doi:10.1021/ja048165l.

369